Initiation of a Solitary Wave Family in the Demise of a Nocturnal Thunderstorm Density Current

RICHARD FULTON*

Cooperative Institute for Mesoscale Meteorological Studies, University of Oklahoma, Norman, Oklahoma

DUSAN S. ZRNIĆ AND RICHARD J. DOVIAK

NOAA/National Severe Storms Laboratory, Norman, Oklahoma

(Manuscript received 15 February 1989, in final form 10 August 1989)

ABSTRACT

This paper describes the characteristics and evolving nature of a vigorous thunderstorm density current very early in the morning of 9 May 1981 in Oklahoma. Because the ambient lower atmosphere was stratified, interesting interactions between the outflow current and the ambient environment resulted. The leading portion of the current was modulated by at least three gravity wavelike perturbations of horizontal spacing 12 km which initially coexisted with it. However, as the current evolved, it initiated an undular borelike disturbance which propagated ahead into the stable boundary layer, carrying cold outflow air in large amplitude rolls. Eventually the wave family left the decelerating outflow air in its wake. This borelike disturbance resembles the Australian "morning glory" phenomenon and appears to represent an early stage in the development of a solitary wave family.

The observations resemble other reported morning glories and solitary waves as well their laboratory and numerically simulated counterparts. Comparisons are discussed. This case study is unique not only because it combines Doppler radar, tall tower, and surface mesonet observations, but especially because the period of observation captures the disturbance in its formative stage when it is still very near the density current.

1. Introduction

Thunderstorm outflows and their associated gust fronts have been studied in many papers in the literature. Observers using an instrumented tall tower have documented the small scale kinematic and thermodynamic structure in the lowest several hundred meters (e.g., Charba 1974; Goff 1976, 1977) whereas Doppler radar has provided kinematic information through the entire depth of the current, which may be one kilometer or more, as well as above it (Wakimoto 1982; Zrnić and Lee 1983; Mueller and Carbone 1987).

Laboratory simulations of these density (gravity) currents have also been performed using relatively dense salt solutions released along the lower boundary of fresh water tanks. Simpson (1969) and Charba (1974) have shown that thunderstorm cold outflows are dynamically similar to these laboratory currents. The laboratory models of Middleton (1966), Simpson (1972), Britter and Simpson (1978), Simpson and Britter (1980) and others have been compared with real atmosphere outflow observations, and resemblance in many aspects has been demonstrated.

Numerical models have provided a unique opportunity to study density current dynamics as well. Most are two-dimensional in the vertical plane (e.g., Mitchell and Hovermale 1977; Thorpe et al. 1980; Droegemeier and Wilhelmson 1987; and Haase and Smith 1989a,b).

One aspect lacking in many of these models is the inclusion of static stability in the environment. Although a tremendous amount of information has been learned about density current dynamics without the inclusion of ambient stability, interesting wavelike phenomena are frequently observed to occur in its presence. Numerical and laboratory modeling efforts directed at understanding these phenomena have increased significantly within the past several years (e.g., Crook and Miller 1985; Haase and Smith 1989b; Wood and Simpson 1984; Rottman and Simpson 1989). They have demonstrated, and observations have substantiated, that density currents such as those initiated by cold thunderstorm downdrafts can induce bouyancy waves in the lower troposphere where stability is frequently enhanced through nocturnal radiation from the earth's surface. These waves often assume the form of internal undular bores and/or solitary waves. They

* Present affiliation: General Sciences Corporation, Laurel, MD.

Corresponding author address: Richard Fulton, NASA Goddard Space Flight Center, Code 612, Greenbelt, MD 20771.

may be identified as long, shallow, quasi-periodic roll clouds, which are observed frequently in the early morning hours in the Gulf of Carpentaria region of Australia and have been called "morning glories" (Smith 1988).

One of the most poorly understood aspects of these phenomena is the nature of their forcing mechanisms and the sequence of events which occur during their formation. Although density currents have been identified as forcing mechanisms, the lack of existing observations during the early formation period has not permitted this problem to be addressed in detail. With this justification the following observations are presented.

The subject is the thunderstorm outflow event occurring around midnight on 9 May 1981. The accompanying gust front originated from a line of thunderstorms which developed in southwestern Kansas during the evening of 8 May. GOES satellite images show that the storms moved rapidly eastward, and new storms developed on the southern end of the line. This new convection accelerated ahead of the original line in the classic "bow echo" fashion and produced strong surface winds near Gage, Oklahoma (GAG; see Fig. 2 for location) which resulted in one death, multiple injuries and significant property damage (NOAA *Storm Data* 1981). The vigorous density current emanating from these storms moved southeastward into the stablizing lower atmosphere over the central and southern part of the state in the early morning hours.

As this gust front passed through central Oklahoma, data were collected from a variety of instruments operated by the National Severe Storms Laboratory (NSSL) in Norman. Measurements from a Doppler radar, a 444 m tall tower, and a surface mesonet were synthesized to provide a composite picture of the evolving outflow. Since the lower atmosphere into which it moved was statically stable, it offered a unique opportunity to analyze its influence on the outflow and vice-versa.

2. Data sources

The major data sources used are: a 10-cm Doppler radar located at Norman, a 444 m instrumented tower, a Stationary Automated Mesonet (SAM), and standard National Weather Service (NWS) rawinsondes. Each of these provides an independent and complementary measure of the kinematic, dynamic, and thermodynamic structure of the outflow and its environment.

The Doppler radar provides, most importantly, wind information in a plane normal to the gust front through a depth exceeding that possible with tower measurements alone. It is along the normal direction that the kinematic and thermodynamic gradients are most significant, and this fact allows a simplification of the continuity equation to permit calculation of the vertical wind component using radial velocity measurements collected normal to the front. Vertical velocity is calculated by first averaging the radial velocities over a narrow five degree azimuth sector normal to the front and then integrating the continuity equation upward. The derived vertical component is then vectorially combined with the radial component to obtain a wind vector in the vertical, front-normal plane. The effects of advection during the data collection period (i.e., a PPI volume scan) were evaluated by simply advecting radial velocity data points back by the speed of the gust front before integration. It was found, however, that there was not a significant change in the deduced flow, mainly because the strongest forcing for the vertical motion is located in the lowest one or two elevation angles.

The tower provides important thermodynamic and corroborative wind information through the lower 444 m of the boundary layer. This data has proven very important to the analysis and interpretation of the events associated with the gust front passage. The data include wind speed and direction, dry- and wet-bulb temperature, and pressure at 10 second intervals. It is instrumented at seven levels: surface, 26, 45, 89, 177, 266, and 444 m. Wind direction, speed, vertical velocity, and dry-bulb temperature are recorded at all of these levels. Wet-bulb temperature sensors are mounted at the surface, 89, 266, and 444 m levels. Pressure is recorded at the surface and top levels. Rainfall is also recorded. The tower is located at an azimuth of 356° and range of 37 km relative to the Norman radar.

Finally the surface mesonet sites provide measurements over an area with sufficient density to allow conclusions to be made as to the evolution of the front. The average station spacing is about 10 km, and the maximum breadth of the network in the front-normal direction is about 55 km. They are located northwest of Norman and provide dry- and wet-bulb temperatures, wind speed and direction, pressure and rainfall averaged over one minute periods. See Fig. 8 for the locations of these instruments.

3. Atmospheric sounding profiles

The closest NWS rawinsonde station to NSSL in central Oklahoma is located 20 km to the northwest at Oklahoma City (OKC). The gust front passed Norman shortly after 0100 (all times are Central Standard Time; CST = UTC − 6 h), and the most representative prefrontal sounding available was at 1800 CST, 8 May (0000 UTC 9 May), about 7 hours earlier. This profile has been adjusted in the lowest one-half kilometer by inserting tower winds and temperatures averaged over a five minute period one-half hour before frontal passage.

Shown in Fig. 1a is the prefrontal virtual potential temperature (θ_v) profile. The stability, as evidenced by increasing θ_v with height, is illustrated, especially below 2–3 km. A profile of Brunt-Väisälä period, $P = 2\pi/N$, (Fig. 1b), where

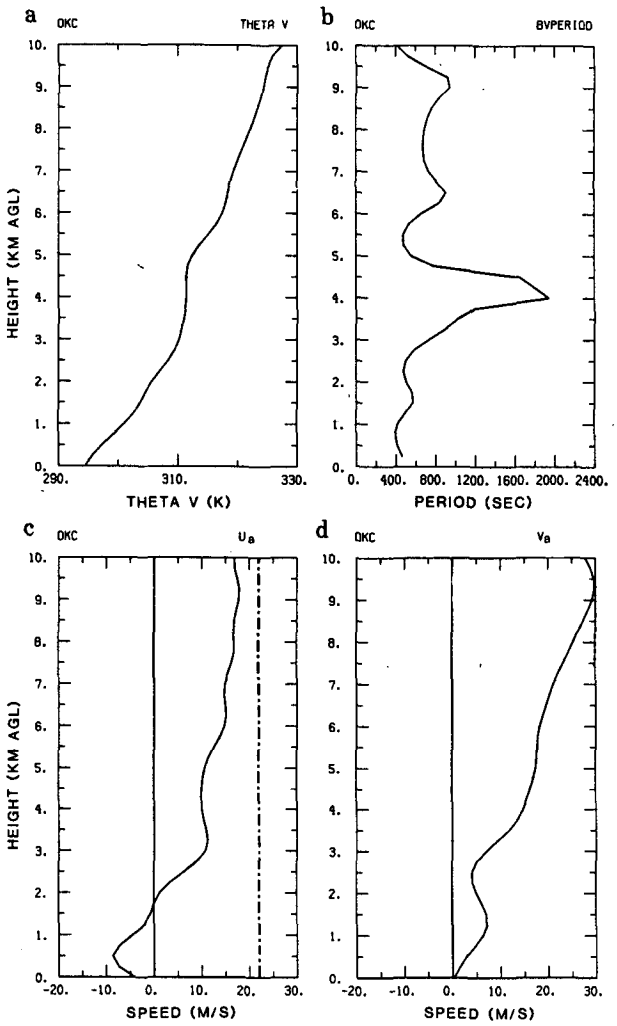

FIG. 1. Oklahoma City, Oklahoma (OKC) soundings for 1800 CST, 8 May 1981 (0000 UTC, 9 May). The lowest 500 m of data have been replaced using the tower data one-half hour before frontal passage. Shown are (a) virtual potential temperature, (b) Brunt–Väisälä period, (c) component of wind speed normal to front and (d) parallel to front. The vertical dash-dot line in (c) marks the gust front speed.

$$N^2 = \frac{g}{\theta_v}\frac{\partial \theta_v}{\partial z} \qquad (1)$$

shows that the smallest periods (highest static stability) occur in the lowest few kilometers with a near neutral layer extending from 3 to 5 km. In still air, low level stability capped by a layer of neutral stability traps boundary-layer wave disturbances because it inhibits the vertical propagation of energy.

The prefrontal atmosphere up to an altitude of 2 km is saturated and characterized by high equivalent potential temperature, θ_e (not shown). Above this, θ_e drops sharply as the mixing ratio decreases from a peak value of 11 g kg^{-1} at the surface to 1 g kg^{-1} at 2 km altitude. The effect of moisture in the atmosphere on borelike wave disturbances is not significant although it can play some minor role in influencing the wavelength and amplitude of the disturbance (Crook 1986).

The wind speed in a coordinate system rotated such that the positive x-axis is oriented toward the direction of frontal motion (to the southeast) is shown in Figs. 1c and 1d. The front-normal component of the ambient wind (U_a) is the one which controls the wave guidance properties of the environment. The prefrontal U_a has considerable curvature within the lowest 3 km with a strong jet of 10 m s^{-1} directed opposite to the gust front motion at 0.5 km altitude. This feature has been shown to inhibit the vertical propagation of energy (Crook 1988), and this will be discussed in more detail in section 7c.

4. Vertical kinematic structure

This section describes the Doppler radar-derived winds associated with the thunderstorm outflow. The motivation here is to discuss the circulation in the vertical plane normal to the gust front. Five sector volume scans of the approaching outflow were collected by the Norman radar (NRO) from 2350 8 May to 0050 9 May at 15 minute intervals; however only one of these will be discussed here. The front was approaching the radar from an azimuth of about 300°. The heavy precipitation associated with the thunderstorm line (peak reflectivity ~ 65 dBZ) moved eastward and remained north of Norman while the cold outflow airmass moved southeastward (Fig. 2). There was no rainfall recorded during the gust front passage at the mesonet stations (see the stippled region in the quadrant northwest of

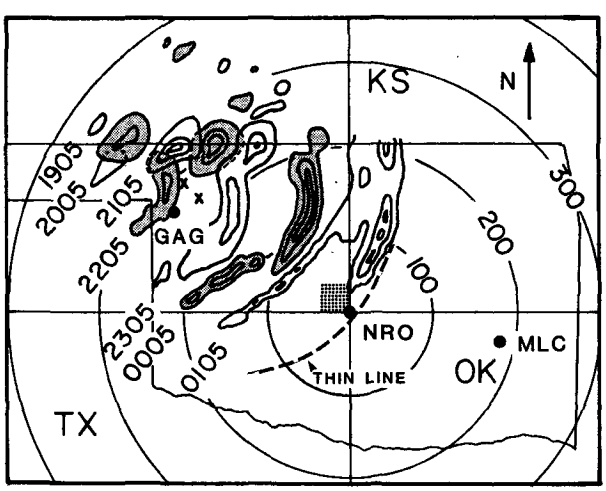

FIG. 2. Sequence of reflectivity contours from NSSL's WSR-57 surveillance and Doppler radars at Norman at one hour intervals. Contours are 35, 45, and 55 dBZ, and alternate times have been stippled. The square stippled region just northwest of NSSL (NRO) represents approximately the area of the mesonet. The two X's in northwest Oklahoma identify reports of high winds and property damage. Range rings are in kilometers.

NRO in Fig. 2) which were all located just south of the southern end of the thunderstorm line.

Figure 3 is a vertical cross section normal to the gust front at 0034. The radar is located beyond the left edge of the figure, and the front is moving toward the left. The cross section is oriented approximately along the 300° azimuth, i.e., southeast to northwest. Ground-relative wind vectors are shown in the top panel, and front-relative vectors are shown in the middle panel. "Front-relative" implies relative to the windshift line (i.e., gust front) which, from a least squares fit to the mesonet data, was determined to move at 22 m s^{-1}. Finally, the bottom panel presents the reflectivity and spectral width structure through the front.

There was a well-defined thin line of reflectivity located at the gust front and extending for nearly 200 km along its length. Its location at 0105 is marked by the dashed line in Fig. 2. The thin line is a relatively common radar reflectivity signature of gust fronts and has been attributed to Bragg reflection from refractive index irregularities and/or insects, leaves or other debris lifted by the frontal updraft (e.g., Ligda and Bigler 1958; Atlas 1960; Wakimoto 1982). The reflectivity associated with the thin line is relatively low, generally about 15 dBZ. It is clearly evident in Fig. 3c at the 42 km range, however the peak reflectivity is only about 5 dBZ at the azimuth shown here. Although it peaks at an altitude of one kilometer, it is still clearly visible at other elevations to an altitude of 3.5 km. The enhanced region of reflectivity centered at 54 km is caused by a small line of weak reflectivity cells which have developed in response to convergence at the front. These isolated cells (not shown in Fig. 2) did not produce the outflow, and they lag the gust front by an ever increasing distance.

High Doppler spectral widths are shaded in Fig. 3. Highest widths (resulting primarily from turbulence on the scale of the radar resolution volume) are located just ahead of the front in this cross section although PPIs indicate that this was not always the case. There are also scattered areas of high spectral widths within the outflow.

The outflow current is made visible by the strong velocities below about 1 km altitude directed toward the left in the top panel; the peak radial velocity is about 25 m s^{-1}. The prefrontal winds at low altitudes are opposing the front. At heights about 3 km AGL, strong westerly winds are detected ahead of the front and are identified by the long vectors directed toward the left. The gust front is clearly delineated by a 5 km wide region of rising motion from 42–47 km range (Fig. 3). The derived peak vertical velocity in the frontal zone is about 15 m s^{-1} at this time and decreased in later volume scans. The maximum reflectivity within the thunderstorm line also decreased with time indicating that the storms were decreasing in intensity. We

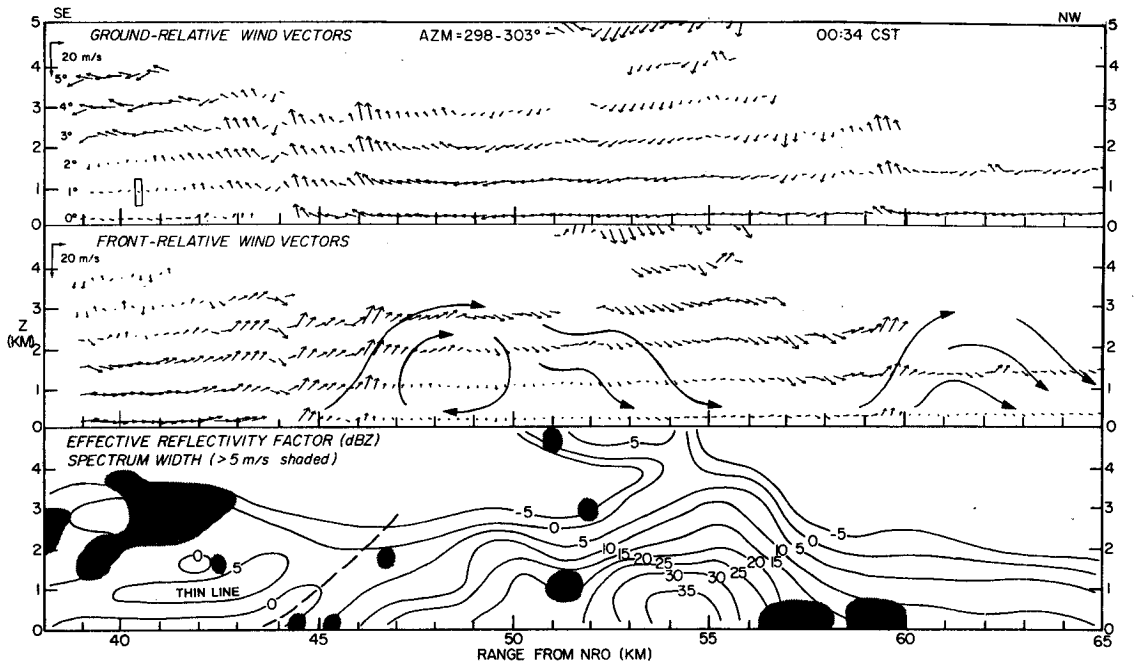

FIG. 3. Vertical cross section normal to the gust front of ground- and gust front-relative wind vectors, and reflectivity and spectral width at 0034 as a function of range from the Norman Doppler radar. Vectors are plotted at every range gate along the appropriate elevation angles. Partial beam blockage at the lowest elevation angle would increase the height of the plotted vectors by 100–200 m. Data are averaged over a 5 degree azimuth sector (298–303°). The box at the lower left of the top panel is the approximate size of the radar resolution volume. Southeast (northwest) is toward the left (right).

suspect that the derived positive vertical velocities may be too large based on comparison with tower vertical velocities. This may result from the accumulation of errors during upward integration of the continuity equation and uncertainties associated with advection as discussed earlier. The net result is that the vertical circulation may appear to be "stretched" upward too high. We suspect that, in reality, the depth of the roll circulation located at 49 km may be overestimated by as much as a factor of two. The qualitative nature of the flow still remains unchanged however.

Another representation of the air flow is shown by the gust front-relative cross section. The updraft is evident, lifting low altitude ambient air to heights of a few kilometers. The upward protruding "head"-like structure, characteristic of density currents, is seen as the 5 km wide rotor at 49 km range. This is similar to the observations of Wakimoto (1982) and Mueller and Carbone (1987). The most unusual feature, however, is the relative motion toward the right at low levels, *opposite* to the direction of motion of the density current. This contradicts the notion of a density current which must have fluid moving at least as fast as the front itself; otherwise the front would become detached from its feeder flow. The only region where the front-relative winds are directed toward the left, and thus greater than the gust front speed, is within the rotary headlike circulation at 49 km. This implies that even though there is a current of outflow air moving to the southeast (in a ground relative sense), as shown in the top panel, the only place where it is being advected *at the gust front speed* is primarily in a narrow 5 km wide zone just behind the gust front.

How is it possible that a gust front can move faster than the density current behind it? In order to answer this it is important first to clarify the meaning of "gust front". The classic definition of gust front describes a sharp increase in wind speed coincident with a sustained windshift and temperature drop. A temperature drop implies a change of airmass. The words "gust front" by themselves, however, only imply a discontinuity in wind *without regard to a change of airmass*, and it is this definition that is adopted in all discussions in this paper. Having established this premise it is suggested here that the gust front is associated with a borelike wave initiated by the cold outflow, and it is moving at a speed which is overtaking the outflow current.

Another feature which raises curiosity is the "secondary front" evident in Fig. 3 at a range of about 60 km with its associated rising motion. Secondary fronts, occasionally observed with thunderstorm density currents, are characterized by sharp, sustained increases in wind speed within the current, however, in this case, the increase in wind speed is short-lived. The relative flow in the middle panel indicates that there is not a clearly defined closed circulation as observed in the first wavelike perturbation at a range of 48 km; therefore there is little or no advection of cold fluid in the gust front-relative frame-of-reference by this second disturbance.

The closely spaced (1–2 km) periodic vertical motion features in Fig. 3 at ranges 42–46 km embedded within the frontal updraft are a result of boundary-layer waves of unknown origin. Close examination of radial velocity PPIs at low elevation angles reveals that these prefrontal waves are oriented at an oblique angle to the front and therefore are not believed to be dynamically associated with it because of their relative orientation.

In order to better understand the low altitude horizontal velocity structure, the radial velocities are plotted in Fig. 4 as a function of range for the lowest elevation angle which went into the construction of Fig. 3. The radar beam axis is at an altitude of about 0.3–0.4 km AGL at these ranges. The gust frontal zone is readily apparent at ranges of 42–48 km; positive radial velocities (away from the radar) change sharply within a 5 km wide zone to strong inbound velocities. This high shear zone is characterized by shear values of 7 $\times 10^{-3}$ s^{-1} averaged over the entire frontal zone with higher local values. However, behind this zone three regularly-spaced surges are evident, each with a decreasing amplitude. By comparison with Fig. 3 the first surge at 48 km range coincides with the rotary circulation. The second surge at 61 km coincides with the "secondary front". The third one at 74 km is beyond the data shown in Fig. 3. These surges appear to be an amplitude ordered sequence of evolving solitary waves.

5. Tower observations

a. *Time series measurements*

Figure 5 shows the front-normal component of wind speed at the 444 m tower level (solid line), and superimposed over this is the Doppler radial velocity plot from Fig. 4 (dashed line) which has been stretched horizontally so that the surges approximately match those observed at the tower. The height of the radar beam (~0.4 km) at the ranges shown is near the 444 m tower level. The three surges observed by the radar are also

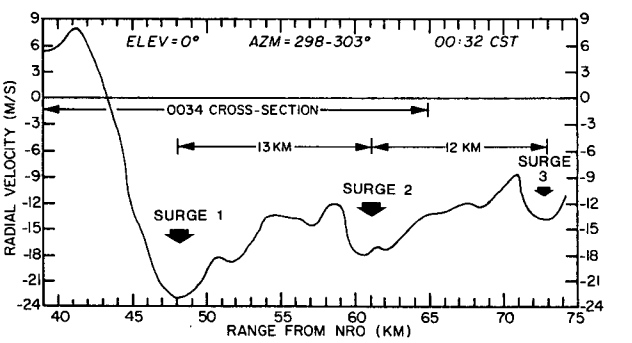

FIG. 4. Profile of radial velocity as a function of range normal to the gust front at 0032 CST and at 0.0 degrees elevation. Velocities have been averaged over a 5 degree azimuth sector (298–303°).

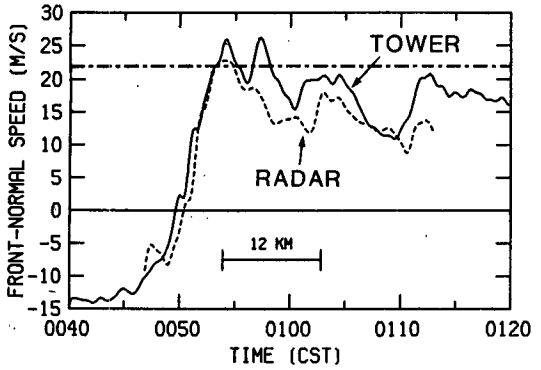

FIG. 5. Profile of the front-normal tower wind speed component at 444 m along 305° azimuth (solid line). Superimposed is the front-normal Doppler radial velocity profile from Fig. 4 (dashed line). The horizontal dash-dot line delineates the speed of the windshift line/gust front.

clearly evident in the tower measurements. The correspondence is quite surprising considering the fact that the tower measurements were taken over a period of 40 minutes while the radar data were collected almost instantaneously at 0032, about one-half hour before the tower data. Also the radar data are displaced about 30 km from the tower location (see Fig. 8 for location) and represent a radar resolution volume average compared to the point measurements from the tower.

Using the "stretched" distance scale from the radar plot and the time scale from the tower plot in Fig. 5, the average translational speed of the trio of surges was calculated to be 22.5 m s^{-1}. This matches the speed (22 m s^{-1}) which was calculated based on the mesonet data and independently verifies the average speed of the three surges. From this one hour of tower observations, it is thus concluded that the overall disturbance as manifested by the three wind surges is relatively steady over a period of at least an hour.

The front-normal component of wind speed exceeds the speed of the gust front (the horizontal dash-dot line in Fig. 5) only in the first disturbance, and possibly in a small region in the second one. This demonstrates that the gust front is dynamically associated with the advancing waves and not the density current front itself because it is well established through observations, laboratory and numerical models that the cold outflow air moves faster than the density current front. If the wind speed at the top of the tower behind the waves is representative of the true outflow air speed, then the density current front must be moving slower than the gust front. This is indeed the case based on mesonet observations, which will be discussed in the next section.

Figure 6 is a time series plot of kinematic and thermodynamic variables at the surface (7 m) and 444 m tower levels levels over a period of 70 minutes. The gust front passage begins about 0045. It is accompanied by a pressure jump (5.5 mb), equivalent potential temperature drop (5.5°C in only 30 seconds at the 444 m level), wind speed increase (26 m s^{-1}), and windshift

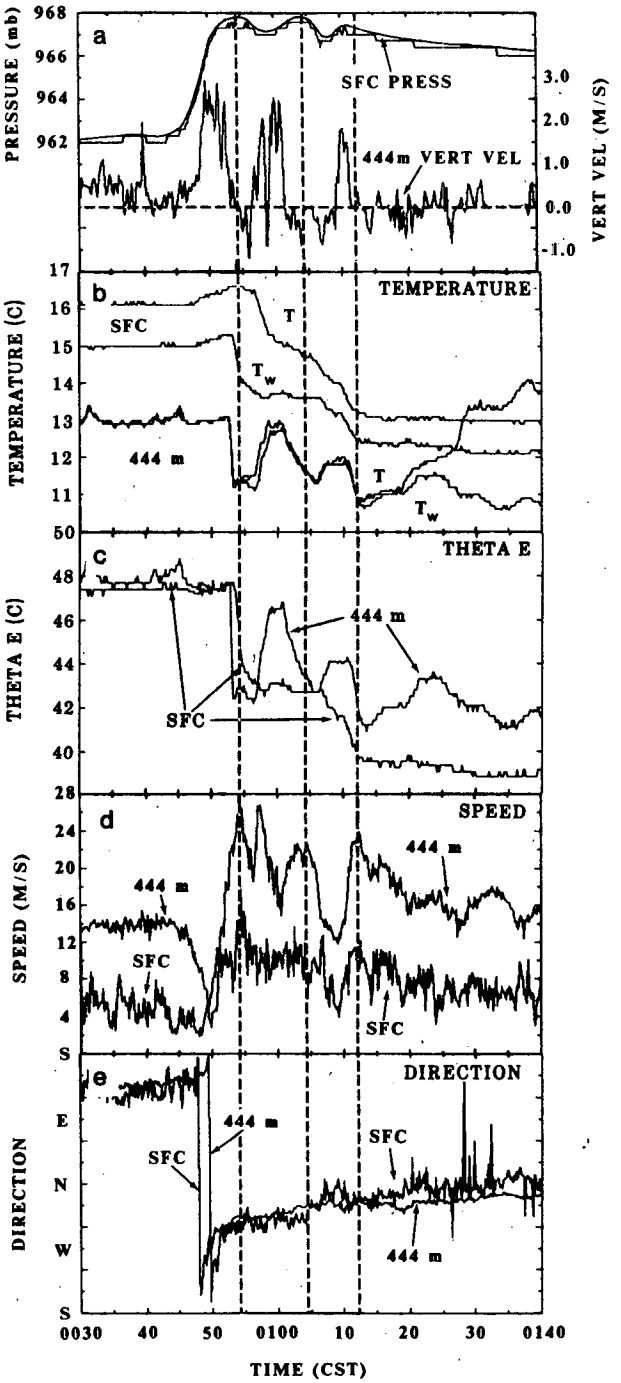

FIG. 6. Time series plots of tower variables at the surface and 444 m levels of (a) surface pressure (raw and smoothed profile) and 444 m vertical velocity, (b) dry- and wet-bulb temperatures, (c) equivalent potential temperature, (d) wind speed, and (e) wind direction. The three vertical dashed lines indicate the center of each of the three wavelike perturbations.

(SE to NW) as is typical of strong gust fronts. The pressure jump begins at about 0046, coincident with a small *rise* in the surface temperature, and the winds shift shortly after this time. The surface temperature doesn't begin to fall until 0057, 11 minutes after the pressure jump and 9 minutes after the surface windshift which, at a propagation speed of 22 m s^{-1}, translates to a spatial scale of 15 and 12 km.

The equivalent potential temperature, θ_e, best locates the leading edge of the change in airmass. The θ_e traces indicate that the cold air mass arrives at about 0053. The pressure begins rising ahead of it while the equivalent potential temperature remains constant; this results in the corresponding prefrontal increase in surface dry-bulb temperature of 0.5°C as shown in panel (b). The calculated rise based on Poisson's equation for potential temperature is 0.4°C.

The most important observation derived from Fig. 6 is the existence of three well-defined disturbances, as denoted by the vertical dashed lines. The time between them is 10 and 8 minutes, respectively. Converting these to distance using the propagation speed of 22 m s^{-1} from the SAM data, one obtains a separation of 13 and 11 km, respectively, which is nearly equal to the distance between surges directly measured by the radar (12 km; Fig. 4).

Figure 7 is a schematic diagram, based on measurements from the tower and radar, at an early stage in the evolution of the disturbance. The shaded region represents the low θ_e air of the cold outflow. The three wavelike perturbations labeled **A**, **B**, and **C** correspond with the vertical dashed lines in Fig. 6. The streamlines are drawn in the frame of reference translating at the speed of the gust front which also equals the speed of the wavelike perturbations. The gust front relative motion is to the right, however it should be made clear that there is still advection of cold air from the thunderstorm in a *ground relative* frame of reference based on the wind field shown in Fig. 3a. Strong rising motion in advance, and weaker sinking motion to the rear, of each individual perturbation results in a net increase in the height of the streamlines as observed with undular bores. The wind surges are located at the inflection points of the vertical velocity trace which implies the existence of a buoyancy wavelike flow.

The surface equivalent potential temperature trace in Fig. 6 drops as the disturbance passes which identifies the cold outflow. The oscillatory temperature change at the tower top (Fig. 6b, c) results from the undular upper surface of the outflow air as illustrated in Fig. 7 which is modulated by the evolving disturbances **A**, **B** and **C**. Adiabatic cooling resulting from rising motion is not the cause for the temporary temperature drops because the prefrontal θ_e values at the surface and 444 m are nearly identical, and thus moist adiabatic ascent (recall that the boundary layer is saturated) will not cause a drop in θ_e at 444 m. The surface pressure responds to the locally deeper outflow air coincident with **A**, **B** and **C** by producing small hydrostatically induced positive pressure anomalies (Fig. 6a).

The outflow air depth is higher than the tower height based on the net drop in θ_e at 444 m (Fig. 6c) and the windshift to the northwest at 444 m (Fig. 6e). However, the near return to the prefrontal θ_e at the 444 m level between **A** and **B** and between **B** and **C** (Fig. 6c) indicates that the outflow depth is about 444 m at these locations. When the current was deeper than the tower height, the depth was estimated by vertically extrapolating the θ_e gradient (based on the data from the four tower levels) until the surface prefrontal θ_e value was reached. The mean depth behind the wave disturbances based on this technique is estimated to be about 0.8 ± 0.3 km as shown in Fig. 7. This is consistent with the depth of strong Doppler radial velocities (Fig. 3). This depth remains relatively constant for at least an hour after the passage of the front.

The surface dry-bulb temperature fall of 3°C is rather small and implies that the outflow air may have mixed with ambient air. The National Weather Service office at Gage, Oklahoma, 240 km northwest of Norman (see

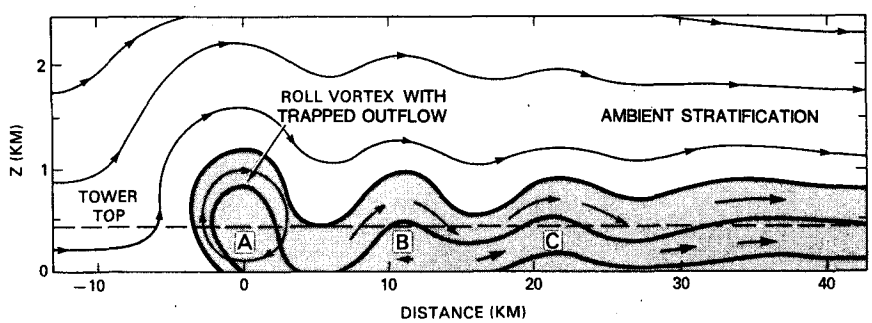

FIG. 7. Schematic diagram of the 9 May 1981 cold outflow disturbance based on tower and Doppler radar observations. The tower sampled the lower portion of the cold outflow current (shaded region) and the radar provided information on the flow fields higher up. The three wavelike disturbances are identified as **A**, **B**, and **C**. The streamlines are in a frame of reference translating with the gust front.

Fig. 2), reported a gust front passage earlier with a surface temperature drop of 8.4°C at a time when the density current is expected to be less modified.

b. Interpretations

The tower time series indicate at first glance the passage of the leading edge of a density current from a thunderstorm downdraft as evidenced, in particular, by the sustained decrease in equivalent potential temperature. However the periodic nature of nearly all of the variables implies that something quite unusual is occurring near this density current's leading edge. There are several interpretations that appear, at least initially, to fit the observations.

Are these wavelike perturbations manifestations of Kelvin–Helmholtz (KH) shear instabilities as observed on the upper surface and near the leading edge of density currents (e.g., Simpson and Britter 1980; Mueller and Carbone 1987)? The KH billow hypothesis is discarded for several reasons, the most conclusive one being that the wavelike disturbances are observed to exist exclusive of the density current as will be shown in the next section. The long-lived quasi-steady nature of the observed disturbance is also evidence against the existence of KH instability.

It is for the same reason that the "multiple surge" interpretation is discarded as well. The atmospheric multiple surge is characterized by apparent multiple fronts *embedded within* an existing thunderstorm cold outflow, i.e., multiple wind and/or temperature discontinuities (Goff 1976, 1977). It has been attributed to the pulsating nature of the downdraft feeding the density current. Similar wind discontinuities in the form of multiple wind surges are observed in the present case; however, the movement of these surges *ahead* of the density current is entirely inconsistent with Goff's multiple surge description.

It is concluded that the observations suggest the coexistence of a disintegrating density current and evolving undular bore. The stratified air flow over the current has resulted in the formation of a borelike wave. A density current which penetrates a stable atmospheric layer and spreads horizontally inside it creates, within the invaded media, a long wave disturbance in the form of a bore which has the length scale of the current. Out of this bore disturbance of long length evolve amplitude ordered waves of shorter length, called solitary waves, with a growth pattern that is controlled by the Benjamin-Davis-Ono (BDO) equation (Christie 1989) and the vertical environmental profiles of wind, temperature and humidity. The decreasing amplitudes of the waves' vertical velocity and horizontal wind perturbations (Fig. 6a, d) support the existence of an amplitude ordered wave family. Furthermore, the separation between the first two waves increases with time (e.g., see pressure trace at SAM 54, Fig. 11) in response to the fact that the larger amplitude first wave is propagating faster than the second wave. This is a characteristic of evolving solitary waves.

The density current is the initiator of the bore, and once this long-wave disturbance on the stable layer is established, the presence of the density current is no longer crucial to the evolution of the undular bore and solitary waves. For example, it has been shown through numerical solutions of the BDO equation that an amplitude ordered sequence of solitary waves evolves out of a long wave disturbance without the concomittent need of an extraneous mass of fluid (Christie 1989). Nevertheless, the density current may be strongly modified by the evolving waves as observed here.

Because the evolving waves may contain large amplitude, closed vortical circulations due to nonlinear effects, they can trap potentially cooler and/or drier air from the current and carry it, at speeds in excess of any speed within the current, beyond what would have been the border of the current in absence of the wave. Thus, cooler air might be present at places where it would not have advected to if the closed waves were not generated, and it could easily give the appearance that the density current front is propagating at speeds faster than that predicted by theory (Benjamin 1968) based upon its depth and temperature deficit relative to the environment. It then becomes difficult to define the density current front. The difficulty in resolving the front is compounded by the fact that the trapped fluid is continually leaking out of the wave and being deposited behind it as the wave propagates ahead of the current as demonstrated in laboratory experiments (Maxworthy 1980; Rottman and Simpson 1989).

It is a simple exercise to estimate this theoretical density current speed which can then be compared with the observed gust front speed. The density current speed relative to the upstream wind (e.g., Charba 1974),

$$V = k\left(gd\frac{\Delta\theta_v}{\theta_v}\right)^{1/2}$$

is estimated from tower data approximately 30 minutes after the gust front passage (and therefore behind the waves) where k is the dimensionless Froude number ranging from about 0.8 (Wakimoto 1982) to the theoretical value of $\sqrt{2}$ (Benjamin 1968), d is the estimated depth of the current (0.8 ± 0.3 km) (see Fig. 7 and associated discussion) and $\Delta\theta_v$ is the mean decrease of virtual potential temperature over the tower depth (3 K; assumed to be approximately equal to the decrease over the entire depth d). The maximum possible density current speed that this equation predicts is 14 m s^{-1}. Subtracting the opposing upstream wind assumed to approximately equal the 444 m tower level wind normal to, and ahead of, the front (14 m s^{-1}; Fig. 5) results in a maximum estimated ground speed for the density current front of 0 m s^{-1}. Although this equation is crude at best since it does not account for ambient

stratification and wind shear, it does provide an estimate which, in this case, is much less than the observed gust front speed of 22 m s^{-1}. This simple comparison supports the earlier statement that the wind shift at the gust front is dynamically associated with a wave instead of the density current front (since the observed depth and temperature deficit in the current would not predict such a rapidly moving gust front) and that this wave is moving ahead of the decaying current. This will be confirmed from direct observations in section 6.

Since we have established the coincidence of the gust front and leading edge of the borelike disturbance, we can now evaluate the degree to which this disturbance is advecting cool air "ahead of the density current front." Recall from past discussion that only in a finite region within the first wave does the current speed equal or exceed that of the gust front. This indicates that potentially cooler air from within the current is being carried along by the first solitary wave. A clear separation of this trapped air from the current would be identified by a surface potential temperature drop followed by a complete return to the prefrontal value after the passage of the first wave, but this is not indicated in the surface θ_e tower data probably because the trapped air is leaking out to the rear as illustrated in Fig. 7. The surface θ_e trace (Fig. 6c) does show, however, a two step drop where θ_e reaches a constant value after the initial sharp drop and just behind the first solitary wave. This may be associated with this leaking air. A secondary sharp θ_e drop at 0106 may locate the "true" position of the density current front (i.e., in the absence of any wave modification), or it may identify cold air carried ahead in the second wave disturbance. There is no conclusive way, in this case, to determine the "true" density current front location other than to estimate the theoretical density current speed as done above, and then assume that any wind speeds exceeding that value significantly are probably dynamically associated with the propagating waves. One could argue that it is not even important to determine this "true" density current front location and proceed to simply define the density current front as the location where the potential temperature begins to fall regardless of the existence of waves. In this case it must be realized that the speed of the density current front may be nonuniform and, at times, greater than that speed predicted by theory if the lower atmosphere can support large amplitude, recirculating wave motion.

It appears as if the density current in this case study is being strongly modified by the stratified flow over it. This is made visible by the development of three wavelike disturbances which initially coexist with the current. Unfortunately the available data do not clearly show the growth of the waves, and the above scenario is deduced both from theory and laboratory results as well as observations. Nevertheless these observations are consistent with the theory of nonlinear waves and furthermore suggest that what appears to be the head of a density current might, in some cases, be cold outflow stripped away from the current and trapped within the closed leading wave of an amplitude ordered train of waves initiated by the density current itself.

6. Undular bore evolution

The most significant contribution of the mesonet data is the documentation of the evolution of the density current and solitary wave family. Figure 8 is a plot of isochrones of the windshift line (i.e., gust front) as it passed through the SAM network. Note the position of the instrumented tower on the northeast side and the Norman Doppler radar (colocated with SAM 1) on the southeast side. The gust front passed across the network essentially as a plane front from the northwest (305°) around 0100 at an average speed of 22 ± 1 m s^{-1}.

The observed speeds of the cold outflow current front (based on the location of the first decrease in surface θ_e) and wave disturbance (based on the pressure jump and wind shift) are plotted using the data from five SAM stations oriented approximately in a line normal to the gust front (Fig. 9), and a least squares line is fit to both. In the last section we concluded that the borelike wave (identified by the gust front) was moving faster than the outflow current based on a comparison between the observed gust front speed and 1) the ob-

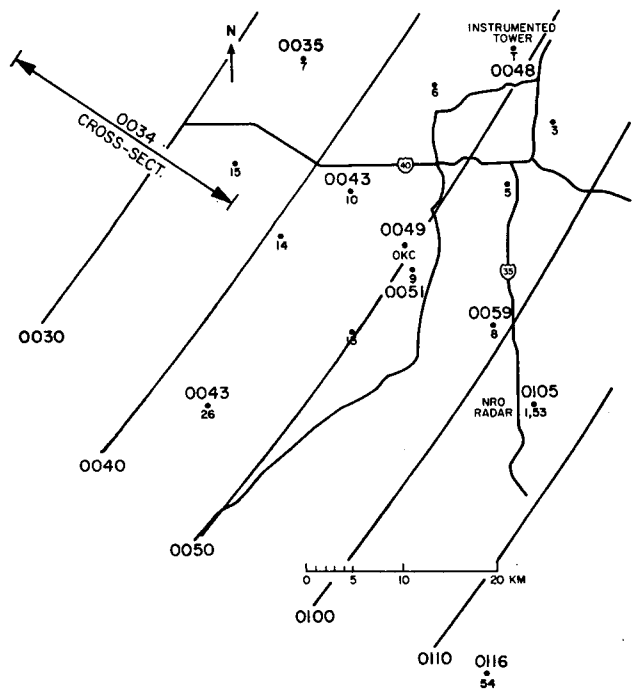

FIG. 8. Isochrones of the windshift over the SAM network. The time (CST) of passage of the windshift is indicated at each station. Also shown is the location of the vertical cross section of Fig. 3.

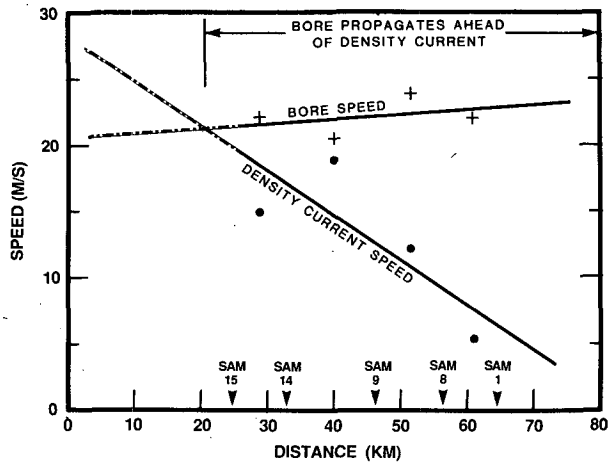

FIG. 9. Speeds of the bore front and the density current front based on data from the five SAM stations oriented in a line normal to the front. The dash-dot extrapolations of the speed lines to the left highlight the uncertainty for locations outside of the network; these two lines, in reality, are probably nearly asymptotic.

served wind speeds within the cold outflow and 2) the calculated theoretical speed of the density current front. The direct observations shown in Fig. 9 confirm this. The speed of the bore is larger than the density current speed at the time when the front is crossing the network. However shortly before it entered the network, the current speed may have been greater than the bore speed based on extrapolation of the curves. This may have prevented the bore from outrunning the current.

In order to illustrate the overall changes which occurred as the wave family and density current traversed the network, the SAM data for two stations spaced far apart will be presented. The two stations are SAM 7, the first to experience the gust frontal passage at 0035, and SAM 54, the last station, at 0115. They are spaced about 50 km apart in the direction normal to the gust front.

These two stations are rather widely separated along the *length* of the disturbance as well. Smith and Morton (1984) have observed that there can be significant variations in bore structure at a single time as one moves along its length. Analysis of our mesonet data reveals some such variations, but much more significant changes occur as a result of time evolution.

Figures 10 and 11 show the time series spanning a three hour period. At SAM 7 there is a pressure jump of 5.3 mb coincident with a windshift and wind surge. Post-jump pressure oscillations of magnitude about 0.5 mb are barely resolved because of the quantization interval of approximately 0.5 mb. Nevertheless two local pressure maxima at about 0041 and 0049 occur nearly simultaneously with two well-defined wind surges, which suggests that they are associated with the evolving solitary waves. This phase relationship between the pressure and wind speed has been well documented from previous observations of solitary waves and undular bores (e.g., Shreffler and Binkowski 1981; Christie and Muirhead 1983; and Doviak and Ge 1984). The equivalent potential temperature drops sharply and nearly simultaneously with the pressure jump indicating the coincidence of the apparent density current front and bore front at this station.

The windshift line passed SAM 54 at 0116, only 41 minutes later, but the traces are very different (Fig. 11). The pressure trace shows a jump with two local pressure maxima and corresponding wind surges as observed with SAM 7, but the magnitude of the pressure jump has decreased to 3.6 mb. However, the most striking difference between the traces at the two stations is the temperature trend. Instead of dropping sharply after the windshift and coincident pressure jump as observed at SAM 7, both the dry-bulb and potential temperatures rise. In fact, the temperature does not fall below the prefrontal value until 60 minutes after the gust frontal passage, at which time a second pressure jump and wind surge occur. Based on sounding data this small warming of the potential temperatures could easily result from vertical mixing of potentially warmer air from above by the propagating wave family as also described in other observations (e.g., Shreffler and Binkowski 1981). The density current front is increasingly lagging the wave family and does not pass the station until about 0215. The near return to the prefrontal pressure before the cold air arrives apparently indicates that the undular bore and evolving solitary waves are now a disturbance dynamically independent of the remnants of the cold air current.

Figure 12 shows the potential temperature plots for each of the five SAM stations oriented in a line normal to the gust front. The leading edge of the density current is defined by the arrowheads at the time when the equivalent potential temperature falls sharply (with the understanding that the "true" location of the density current front may be obscured by the advection of fluid within the waves as discussed earlier). An increasing period of warming ahead of the cold air, caused by vertical mixing associated with the forward propagating wave family, is illustrated.

Figure 13, a similar plot for wind speed, shows that there are at least two, and as many as four (see SAM 8), wind surges immediately behind the pressure jump. Each wind surge is associated with a developing solitary wave. The surges at each station remain a constant distance behind the pressure jump. The existence of the density current is seemingly inconsequential at this stage in the evolution of the waves.

Evidence for partially cutoff outflow air in the first wave is suggested in the θ_e and wind traces for SAM stations 15 and 14 (Figs. 12 and 13). Shortly after the initial θ_e drop there is a brief period of warming which is then followed by a secondary sharp cooling. The wind speed plot for SAM 15 shows that the first periodic wind surge coincides exactly in time with this brief cold anomaly. The second wind surge occurs with the second sharp θ_e drop. At SAM 14, located to the south-

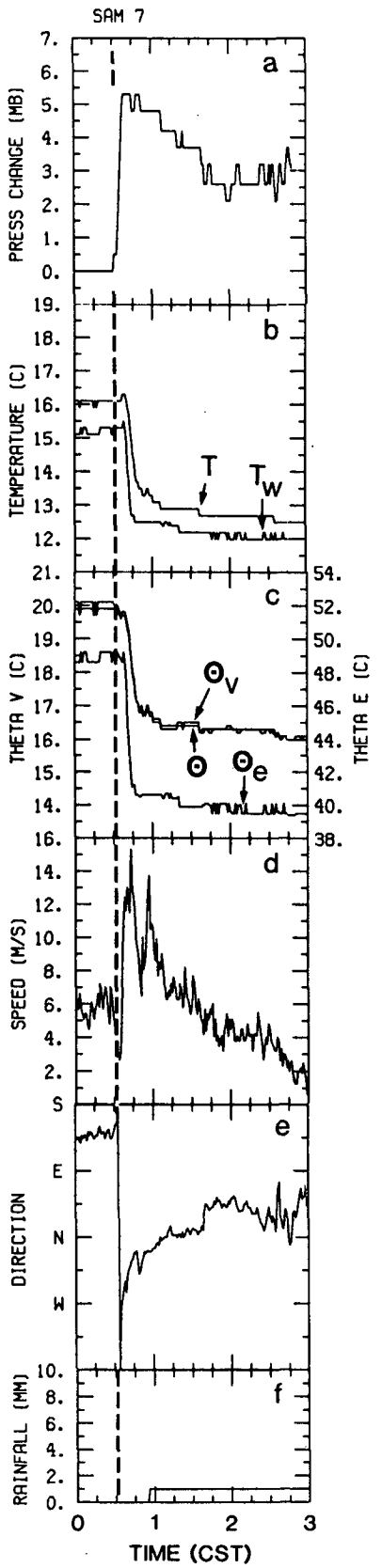

FIG. 10. Time series of variables at SAM station 7: (a) pressure, (b) dry- and wet-bulb temperature, (c) potential, virtual potential, and equivalent potential temperature, (d) wind speed, (e) wind direction and (f) accumulated rainfall. The vertical dashed line marks the time of the pressure jump.

east of SAM 15, the first wind surge lies slightly ahead of the center of the detached cold pool (~2 min) which indicates that the cutoff air is leaking out behind the wave as it propagates ahead. The nonexistence of detached cold air associated with the waves at the other stations suggests that the trapped fluid has completely leaked out of their closed circulations, or that the wave amplitudes have decreased enough that closed circulations are no longer maintained.

The corresponding pressure traces (not shown) illustrate that each wind surge coincides approximately with a small positive pressure anomaly. An interesting observation derived from the pressure data is that these local pressure maxima, each associated with one of the evolving solitary waves, are separating. The time between the first two maxima increases with time; SAM stations 15, 14, 9, 8, and 1 show time separations of 11, 11, 12, 13, and 14 minutes, respectively. This implies that the solitary waves are moving at different speeds, with the first wave propagating faster than the trailing waves as predicted by theory (Christie et al. 1979).

Figure 14 summarizes these observations by plotting the time of passage of significant events at each of the five SAM sites discussed above. The pressure jump occurred first at all stations followed closely by the windshift and dry-bulb temperature increase. Because these lines are relatively straight, the discontinuities are moving at a nearly constant speed, determined earlier to be 22 m s^{-1}. They are followed by the first speed surge and its coincident local pressure peak, trailing the pressure jump by a nearly constant 8 minutes (or 11 km at a translation speed of 22 m s^{-1}), and then the second surge.

The curve delineating the leading edge of the density current shows that the density current front, which was initially located ahead of the first solitary wave, trails the pressure jump (i.e., bore) by an ever-increasing time, from 8 minutes at SAM 15 to 38 minutes at SAM 1. The observations presented in Figs. 10 and 11 for the first and last sites to experience frontal passage show that this trend continues. The second disturbance (SP2, PP2) remains behind the density current front until after it passes SAM 8.

Figure 14 suggests that the disturbance, which initially took the form of a density current, was transformed into a solitary wave family, independent of the decelerating current which eventually came to equilibrium with its environment. The waves initially coexisted with the cold current and, because of their closed circulations, dragged cold air along with them as they propagated ahead, thus resulting in disruption of the density current structure and leading eventually to its demise. The leading edge of the low θ_e air from the

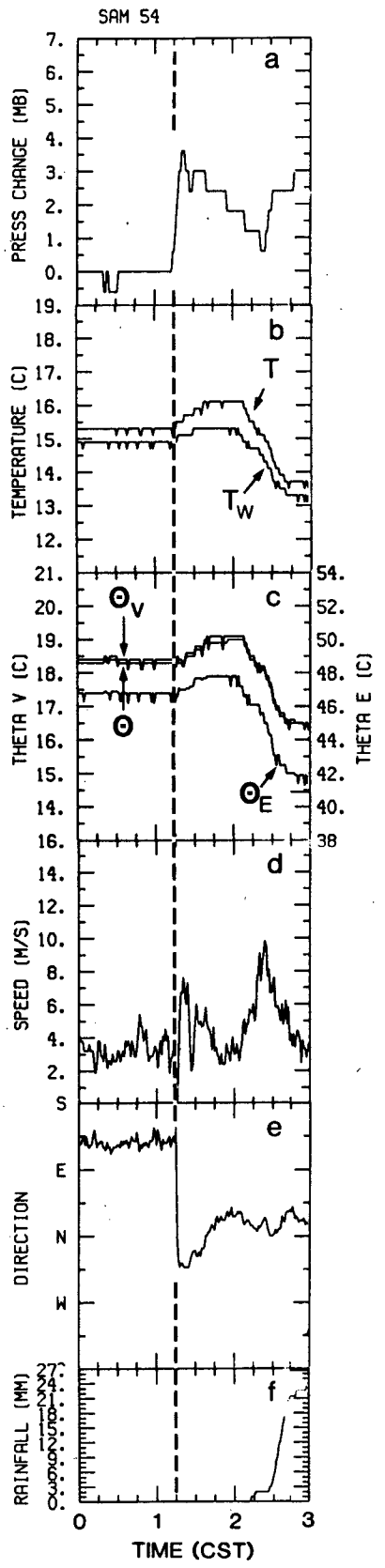

FIG. 11. As in Fig. 10 except for SAM station 54.

outflow current eventually lags the wave disturbances because the cold air which was initially trapped within the closed circulation of the first, and possibly second, solitary wave has completely leaked out behind them as their amplitudes decreased, leaving the wave family to propagate ahead of the cold outflow independently. This has been modeled in the laboratory by Maxworthy (1980) and Rottman and Simpson (1989) and will be discussed in the next section. In agreement with theory, an amplitude ordered family of solitary waves evolved and propagated at a relatively constant speed into the ambient environment, a speed which is determined by the atmospheric density and wind profiles and the amplitudes of the individual waves. This wave front replaces the density current front as the main discontinuity in wind speed, direction and pressure.

Lack of detailed observations after the front passed out of the mesonet to the south and east of Norman precludes any further description of the evolution of the front and bore as the night progressed. The Doppler radar also ceased data collection shortly after the front passed Norman. However, the peak surface wind gust associated with the first solitary wave decreased by 50% (from about 20 to 10 m s^{-1}) during the relatively short time it crossed the network, consistent with a decreasing wave amplitude.

The long term trend of the surface pressure also indicates a decreasing amplitude with time. Analog barograph traces from OKC and McAlester, Oklahoma (MLC) located about 220 km east-southeast of OKC (see Fig. 2 for location) reveal longer term evolution of the disturbances (Fig. 15). The pressure jump associated with the disturbance passed OKC at about 0045 with a magnitude of 5.1 mb; several post-jump oscillations are evident. A pressure jump also passed MLC two hours and ten minutes later, but the magnitude had decreased to 2.0 mb and no oscillations were evident. This trend is reversed to that predicted by theory in which an initially smooth jump steepens and undulations develop (e.g., Christie 1989). The theory however does not include upper level stratification as is typical in the real atmosphere, and therefore it may not realistically predict energy loss. Smith and Morton (1984; Fig. 4) observe a similar trend to that observed here for one of their cases. The surface report from MLC near the time of bore passage indicates that the wind direction was southerly before the bore passage and southerly at the hourly report 55 minutes after the pressure jump passed the station. It is possible that the temporary wind shifts to northwesterly that would be expected with solitary wave passages went undetected between hourly observation times. Two hours after the jump, however, the winds had shifted to northerly, and the temperature fell 2°C, apparently in response to the remnants of the density current.

Turbulent frictional dissipation at the surface has been shown numerically to affect the evolution of solitary waves (Christie 1989). A well-developed solitary wave family can rapidly lose its undular character and

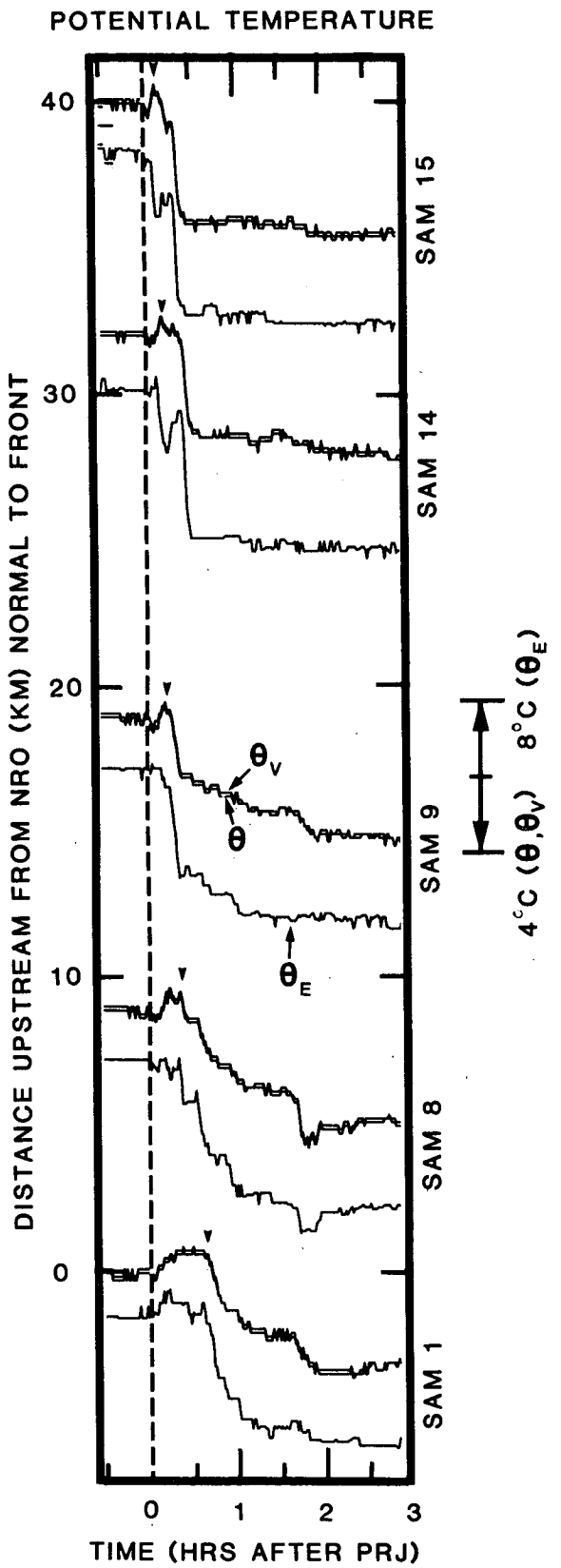

FIG. 12. Time series plots of potential, virtual potential, and equivalent potential temperature for SAM stations 15, 14, 9, 8 and 1 which form a line approximately normal to the front. Each individual plot has been shifted so that the times of the pressure jumps at each station are aligned (dashed line). The ordinate distance scale is relative to Norman (NRO; coincident with SAM 1) and increases to the northwest of NRO. The arrow heads delineate the time when the equivalent potential temperature begins to fall, defining the apparent location of the density current front.

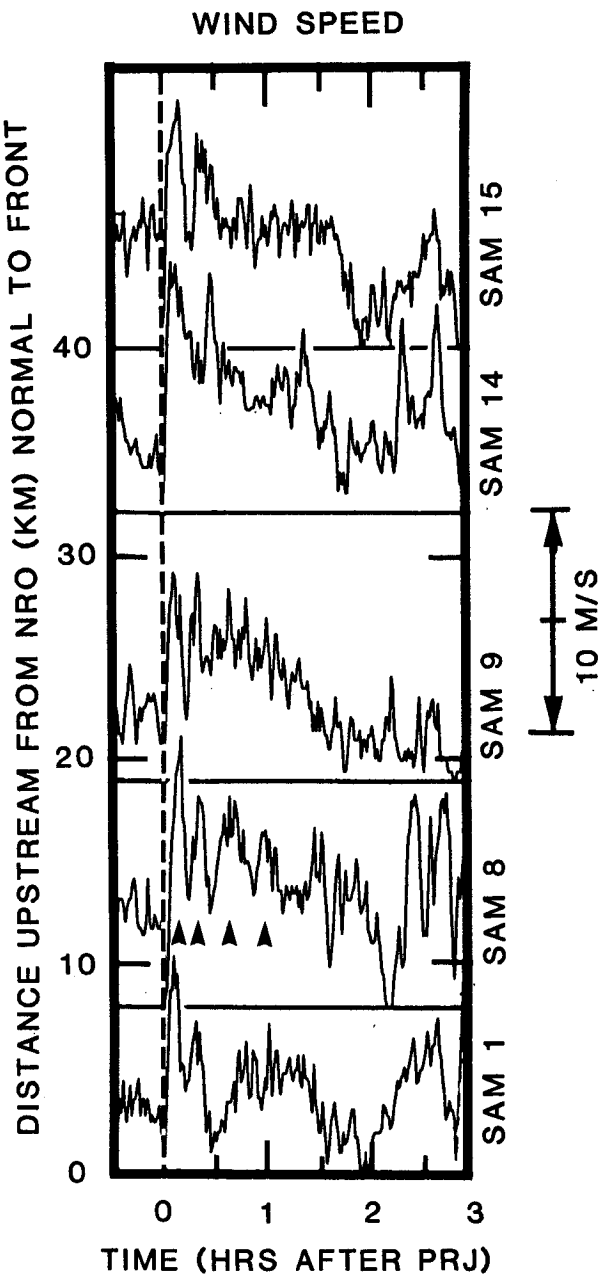

FIG. 13. As in Fig. 12 except for wind speed. The solid horizontal lines represent zero wind speed at each station. SAM 8 experiences four well-defined wind surges as indicated by the arrowheads.

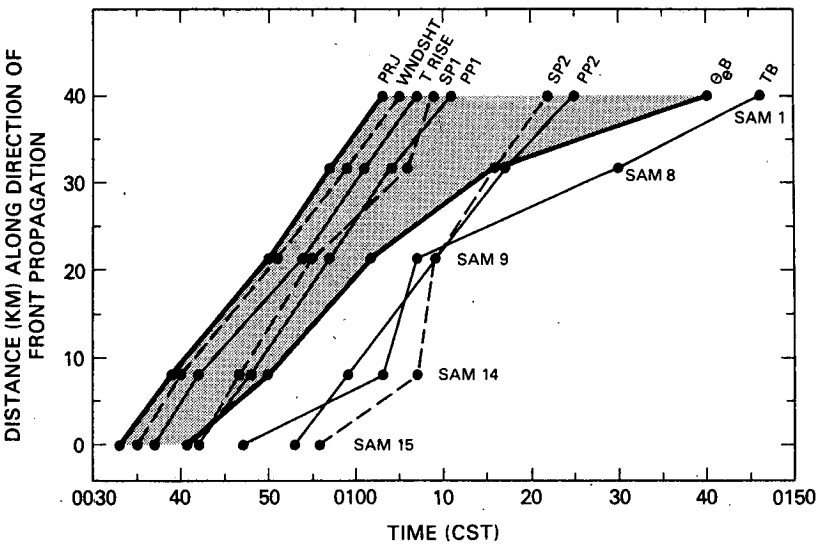

FIG. 14. Composite of the passage of significant events at five SAM stations oriented in a line normal to the front. The pressure jump (PRJ) occurs first at all stations followed immediately by the windshift (WNDSHT), the rise in the dry-bulb temperature (T RISE), the first speed peak (SP1) and pressure peak (PP1), and then the second speed peak (SP2) and pressure peak (PP2). Only the first and second waves are shown since other waves were not as clearly defined in the data for all of the mesonet stations. The leading edge of the density current is delineated by the time when the equivalent potential temperature begins to fall ($\theta_e B$). *TB* defines the time that the dry-bulb temperature falls below the prefrontal value. The shaded region highlights the increasing time between the bore front and the density current front.

amplitude, as depicted in the barograph traces in Fig. 15, with the inclusion of boundary friction. However, radiation damping is probably the most significant mechanism responsible for the observed evolution. The implications of the atmospheric structure in the present case as it relates to radiation damping will be discussed in section 7c.

7. Comparisons

a. Other observations

Probably the best documented example of a pressure jump in close proximity to a thunderstorm density current is the case presented by Charba (1974). This

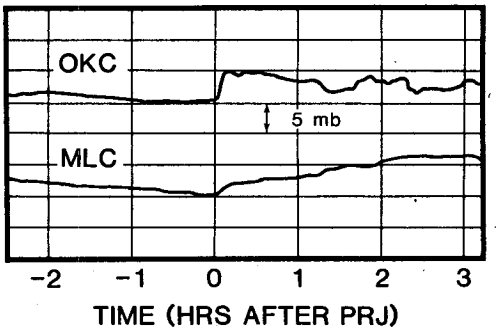

FIG. 15. Barograph traces from OKC and MLC illustrating the decreasing amplitude of the bore as it propagates southeastward. The two stations are separated by about 220 km.

intense thunderstorm outflow event occurred in May 1969 in central Oklahoma and was also observed with the NSSL surface mesonet and tall tower. The similarities between this event and the present case are quite remarkable. Both occurred around midnight local time. Both outflows produced very strong surface winds which originated from an eastward-propagating thunderstorm squall line. Most importantly, both produced a prefrontal pressure jump with periodic wind surges and a periodic vertical motion field.

Figure 16 shows the time series of temperature, wind speed and surface pressure at the tower as the leading edge of Charba's outflow passed. The pressure jump occurred at 2330, 9 minutes before the cold air arrived, and coincided with a shift in the wind direction from south to northwest. The dry-bulb temperature responded apparently to the prefrontal pressure rise by increasing about a half of a degree as in the present case. The cold air front coincided with a strong wind surge of 27 m s^{-1} in the direction of frontal motion and a temporary drop in temperature at 444 m above ground level. There is also a secondary wind surge and temporary temperature drop at 444 m deeper within the outflow. These two perturbations are highlighted by the vertical dash-dot lines at 2339 and 2347 CST. They are each accompanied by a couplet of local maximum rising and sinking motion. The spatial and temporal separation of the two buoyancy wavelike disturbances (9 km, 8 minutes) compares well with the separations for the 1981 case. Recall from earlier

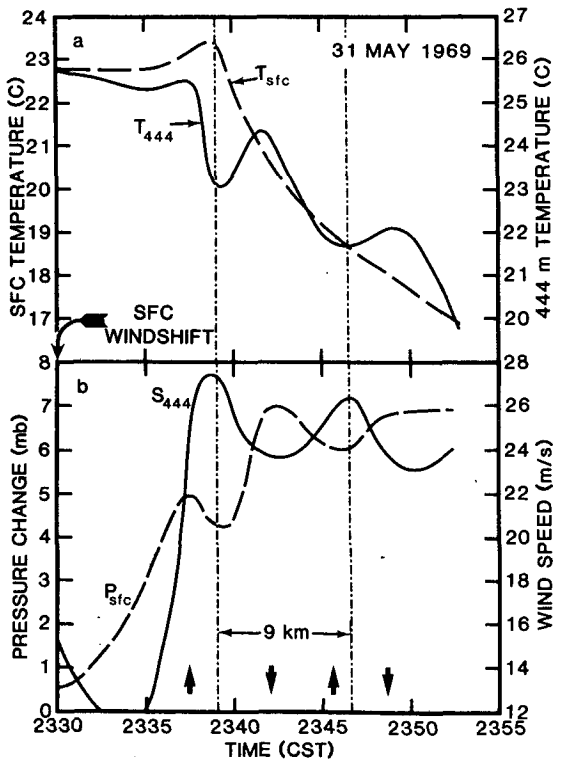

FIG. 16. Traces of (a) dry-bulb temperature at the surface and 444 m, and (b) surface pressure and 444 m wind speed at the WKY tower in central Oklahoma associated with the passage of a thunderstorm outflow on 31 May 1969. The vertical arrows along the bottom of (b) locate the regions of local maximum rising and sinking motion. The two vertical dash-dot lines locate the center of two wavelike disturbances. The periodic trend of the variables is very similar to the 9 May 1981 case. (Adapted from Charba 1974).

discussion that the oscillatory trend of the 444 m temperature for the 9 May 1981 case was attributed to the undular upper surface of the density current. Comparisons with Fig. 6 show that the two events are similar in nearly every detail. Both indicate that the first disturbance is the most intense.

Charba invokes Tepper's (1950) cold front-induced hydraulic jump mechanism to explain the existence of a pressure jump ahead of the density current while downplaying the existence of the secondary wind disturbance. As in the present case the wavelike disturbances observed by Charba coexisted with the cold outflow current. Unfortunately there is no discussion in his paper regarding the evolution and eventual fate of the periodic disturbances. Reexamination of Charba's observations in light of the observations for the present case strongly suggests that his thunderstorm outflow event, which has long been characterized as the "classic" thunderstorm density current, is actually a dissipating density current strongly modulated by a developing solitary wave family as in the present case. It appears from other published observational cases studies that some multiple surge outflow events previously attributed to pulsating thunderstorm downdrafts may be better interpreted as developing solitary waves families.

Scott and Ackerman (1983) describe interesting mesonet observations of another nocturnal, thunderstorm-excited boundary-layer wave disturbance in Illinois. They document a rapidly evolving, although much less intense, cold outflow which again exhibited several features quite similar to the present study. The mesonet stations revealed that the evolving outflow initially was characterized by a singular windshift; but several hours later the outflow exhibited a periodic wind direction trend with the wind direction oscillating three times with a period of 20 minutes between the prefrontal southerly direction and the postfrontal northeasterly direction. This strongly supports the hypothesis that a family of solitary waves has been generated in the demise of the cold outflow current, although the authors did not suggest this as an explanation. This is supported by the fact that initially the pressure jump and windshift occurred nearly simultaneously with the drop in θ_e, but later the θ_e drop lagged 60 minutes behind the windshift. At this later time the three disturbances (identified by the wind shifts and surges) had all moved ahead of the decelerating density current. Soundings indicated the existence of a shallow, surface-based inversion which apparently served as the waveguide. Their observations also strongly support the existence of trapped density current air in the first solitary wave (see Fig. 4 of Scott and Ackerman 1983); a temporary drop in θ_e followed by a recovery and then a more substantial drop is similar to the trend observed in this case. The paucity of cases of undular bores observed in Australia containing trapped air from the density current led Smith and Morton (1984) to conclude that this feature occurs only in the early, formative stages of bores when they are very near their source. Our data support this conclusion.

There are other papers that describe thunderstorm-induced, prefrontal, periodic boundary layer wave disturbances, e.g., Pothecary (1954). These studies present observations of the apparent initiation of solitary waves in the near vicinity of thunderstorm density currents. They provide proof of the ability of atmospheric density currents to initiate boundary-layer wave families, but more importantly they attempt to explain the means by which this occurs, an aspect which is still poorly understood. Other papers describe in detail well-developed wave families and/or undular bores after they have long since outlived their thunderstorm density current source (e.g., Shreffler and Binkowski 1981; Haase and Smith 1984; Doviak and Ge 1984).

In another paper Christie et al. (1979) presented barograph observations of undular surges in Australia, which have evolved from more general density intrusions such as katabatic mountain drainage and sea breeze fronts. Many of these lower atmospheric surges eventually developed into solitary wave families. Measurements from an array of microbarographs suggested

that initially these density intrusions are characterized by a sharp rise in pressure (typically ~1 mb); the post-jump pressure trace is smooth and remains high for an hour or more. If the environment is stably stratified, however, the jump may steepen, and the pressure trace often develops a wavy character behind the jump. As the disturbance evolves, larger amplitude wave components can develop in a relatively short time (1–2 hours, Christie and Muirhead 1983) and dominate the leading portion of the long wave disturbance as theory also predicts.

Clarke et al. (1981) and Clarke (1983) described the kinematic and thermodynamic structure of several undular bore events in Australia which are caused by the inland collision of two sea breeze density currents. Doviak and Ge (1984) presented the first Doppler radar observations of a single solitary wave in Oklahoma caused by a thunderstorm downdraft impinging on a preexisting stable layer laid down by an earlier thunderstorm passage. Their observations suggested that the solitary wave may be carrying cold air from the downdraft within the closed horizontal vortex which is consistent with the interpretations of the present case.

b. *Laboratory experiments*

Laboratory simulation using shallow fluid tanks has aided the understanding of the evolutionary behavior of density currents. Early modeling efforts concentrated on the dynamics of density currents moving within neutral fluids (e.g., Middleton 1966; Simpson 1969; Simpson and Britter 1980). Later, density currents were released into two-layer, stratified fluid systems, and the influence of the current on its surroundings and vice-versa were studied. This is still an active area of research.

Maxworthy (1980) observed the development of multiple solitary waves aligned parallel to the density current front in an experiment in which a dyed, dense current was released into a shallow tank containing static, stratified layers of salt and fresh water. Initially the waves coexisted with the current at its leading edge, modulating its depth. However, as the current slowed down, they were observed to propagate ahead of the current as an amplitude-ordered family. The leading large amplitude waves contained closed, vertical circulations resembling a series of long, horizontal roll vortices, each containing dense fluid from the density current which had been advected along with the waves. The waves eventually decreased in amplitude due to energy dissipation and consequently lost their closed circulations. As a result the advected fluid leaked to the rear and was left behind as they propagated ahead. The evolutionary behavior of the 9 May 1981 outflow is quite similar to this experiment.

Maxworthy repeated the experiment but substituted a neutral, homogeneous fluid for the two-layer, stratified fluid. Waves did not form, but instead the density current exhibited the characteristic "lobe and cleft" structure observed in earlier laboratory experiments. This result may explain the higher frequency of *nocturnal* thunderstorm outflows associated with periodic wavelike, surge-like boundary layer disturbances. That is, the existence of the surface-based, nocturnal radiation inversion (or any other stable layer in the lower atmosphere) is critical to the generation and maintenance of these wave disturbances.

Simpson (1982), Wood and Simpson (1984), and Rottman and Simpson (1989) have addressed the importance of the vertical scale of the ambient stratification relative to the density current depth on the resulting structure of the density current and incipient bore. Simpson (1982) describes the results of two-dimensional laboratory tank simulations in which a dense fluid was released into a stably stratified fluid. Two ambient density profiles were tested, one in which there was a surface-based stable layer with a depth less than the density current depth, and a second one in which the ambient density gradient extends from the floor through a layer deeper than the current. For the first case (a relatively shallow stable layer) Simpson found that if the current flowed at speeds greater than the solitary wave speed, the current was almost unaffected by the stratification. If the density current speed was almost equal to the critical wave speed, a solitary wave with closed streamlines developed. And at subcritical speeds, a train of solitary waves developed and moved along the stable layer ahead of the current.

For the second case of a deep (relative to the density current depth), linearly stratified ambient fluid (which is a closer approximation to the density profile on 9 May 1981), he found that waves formed on the current "which interacted with the current head to destroy the original front and cause a succession of density current heads". His description of this experiment, however, made no mention of waves that propagated ahead of the current. Although the initial conditions for the latter experiment seem to better model the environment on 9 May, the results from the former experiment better reproduce the events which were observed. One could justify, however, a description of the structure depicted in Fig. 7 as a succession of density current heads.

Wood and Simpson (1984) described a similar set of experiments in which the depth of the prefrontal stable layer was varied to determine the effects on the density current. They found that as this depth was increased, the density current itself was progressively transformed into a borelike disturbance with the sharp density current front and turbulent wake region becoming increasingly smooth and undular in form.

Rottman and Simpson (1989) showed experimentally that only for certain combinations of values of relative depths of the density current and ambient stable layer and the relative densities of the fluids can a bore form and move ahead of the current (which acts like a solid obstacle in the flow). The resulting bore can be smooth and undular (Type A), or alternatively it can resemble a density current with a singular jump

and strong mixing in the wake region behind the bore (Type C). Its nature depends on the relative depths of the stratified layer ahead of (h_0) and behind it (h_1). For small h_1/h_0 (<2) the bore is smooth and undular (i.e., wavelike), while for $h_1/h_0 > 4$ the bore resembles a density current with a single steep jump and strong post-jump turbulence. Waves do not form behind the jump in this latter case. In both cases, density current fluid can be carried along by the bore as it propagates ahead of the current. Comparison of these laboratory results with the 9 May observations reveals many similarities, and the laboratory predictions of bore strength are in agreement with the observations. The parameter values discussed by Rottman and Simpson and calculated from our observations fall within the regime which predicts a propagating bore with a smooth and undular structure, and this description matches the observed bore better than does a singular jump with strong wake turbulence.

c. *Numerical models*

This section discusses several relevant numerical modeling studies with the purpose of comparing the general features of simulated density-current-excited solitary waves with those observed in the 9 May 1981 case. The theory behind bores and solitary waves is quite complicated because the relevant equations are nonlinear. Many papers have treated various aspects of nonlinear wave theory in fluids of finite and infinite depth. Benjamin's (1967) deep fluid, nonlinear, dispersive wave theory has been found to describe the essential features of solitary waves (Christie et al. 1978, 1979; Christie 1989) and undular bores (Clarke et al. 1981; Haase and Smith 1984; Noonan and Smith 1985).

Clarke (1984) and Noonan and Smith (1986) simulated the collision of two opposing sea breeze fronts [each using a two-dimensional (x, z) dry, hydrostatic numerical model] and observed the formation of an internal bore in the lower atmosphere. Crook and Miller (1985) presented the first results from a dry, 2-d (x, z), nonhydrostatic model with significantly higher grid resolution to model the generation and evolution of undular bores by a density current. A sequence of waves (as many as four) developed one by one near the density current head and moved ahead into the stratified, two-layer environment. They were ordered by amplitude as theory predicts and as observations from the 9 May case support.

However, there are several major differences between these model results and the observations which may be explained by the differing ambient vertical density and/or wind profiles. Large amplitude, closed circulations within the leading waves, associated with strong nonlinear effects, did not develop in the simulations. Also the modeled waves did not alter the structure of the leading edge of the density current as in the observations, i.e., they did not modulate the density current depth and kinematics. Instead they formed near or just ahead of the current head, one at a time, and subsequently propagated ahead without clearly interacting with the density current. Because they formed ahead of the current and did not have closed circulations, it was not possible for them to transport cold outflow air.

Later Crook (1986, 1988) used the same model to determine the effects of deep stratification and vertical wind shear on bores. Earlier work assumed a static, neutral atmospheric stability profile above the boundary layer which prevents the upward escape of energy. His results showed that stability through a depth greater than just the boundary layer, as in the real atmosphere, significantly reduced the amplitude of the bore by allowing energy to propagate upward. In the present case, since there is not a deep neutral layer above the low altitude stratification, there must be some other mechanism. Crook found that certain vertical wind profiles can also lead to trapped energy, such as a strong winds at upper levels opposing the wave motion. This feature, however, does not exist in the prefrontal sounding as ($U_a - c$) decreases with height (Fig. 1c). A second mechanism, which Crook discusses, is a strong low level jet that opposes the wave motion. This feature does exist for this case. Intrinsic in the existence of a low level jet is strong curvature in the wavenormal wind speed, U_a, above the jet which can result in an imaginary Scorer parameter, l, where

$$l^2 = \frac{N^2}{(U_a - c)^2} - \frac{U_a''}{U_a - c},$$

c is the wave speed, N^2 is defined in (1), and U_a'' is the curvature of the wavenormal ambient wind. A profile of l^2 is shown in Fig. 17. Below 3 km altitude there is a general decrease of l^2 with height, and it becomes negative from 3–4 km. This results in trapping of energy at low levels and probably explains why the observed wave disturbance was maintained for several periods.

Haase and Smith's (1989b) 2-d (x, z) model results are quite similar to our observations and describe the initiation of a borelike disturbance by a density current. They show that the speed of the density current, c_g, relative to that of infinitesimal amplitude long waves on the prefrontal stable layer, c_0, is important in the characterization of the disturbance which develops. The c_0 depends on the depth and stability of the prefrontal stable layer; the deeper the layer and/or the higher the Brunt-Väisäilä frequency within the layer, the larger is c_0. For a small value of c_0 relative to c_g, the density current moves faster than any waves which may be generated, and therefore no prefrontal disturbance can exist; however the structure of the current head is modified. As c_g decreases (as would be expected in the real atmosphere as the current depth decreases with time) the current head becomes separated from the body of the current and resembles a large amplitude wavelike disturbance, advecting cold air in a closed

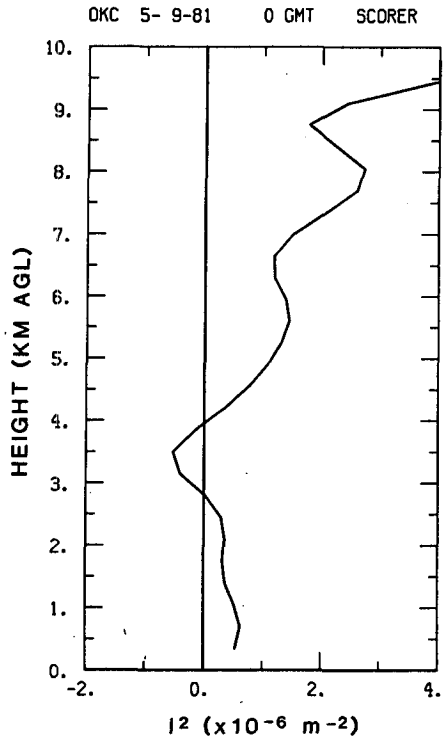

FIG. 17. Square of the Scorer parameter, l^2, calculated from the modified 1800 CST, 8 May 1981 prefrontal sounding in Fig. 1.

vortex. This wavelike vortex continues to move ahead of the current, and other waves (with successively smaller amplitudes) are formed.

8. Summary and conclusions

Single Doppler radar, tall tower, and surface mesonet observations are presented for one nocturnal cold outflow event in Oklahoma on 9 May 1981 that was generated by a thunderstorm squall line. Surface observations reveal that this cold outflow has many features of a density current, i.e., the current front is characterized at the surface by a nearly coincident pressure jump, windshift, wind speed increase, and temperature drop. However, a particularly unusual aspect is the existence of three periodic wind surges initially embedded within the leading portion of the current with spatial and temporal separations of 12 km and 10 minutes, respectively. Tall tower measurements show that each of these surges is associated with a couplet of rising and sinking motion, a local minimum in the 444 m potential temperature, and a small, hydrostatically induced, local maximum in surface pressure. These buoyancy wavelike perturbations embedded within the density current result from the forced motion of the stable nocturnal boundary layer air over the current.

Over a relatively short time the cold density current decelerates and, in doing so, allows the undular bore to propagate ahead at a nearly constant speed of 22 m s^{-1} into the prefrontal boundary layer carrying cold air from the current in large amplitude roll circulations. This cold air eventually leaks out as the wave amplitude decreases. This disturbance appears to be a developing family of solitary waves and is characterized at the surface by a sharp increase in pressure and wind speed, and a wind shift. The first wave has the largest amplitude in agreement with the theory of solitary waves. The period of observations has captured their early formative stage. Supporting conventional data reveals that this wave family continues propagating southeastward for at least several more hours as an independent disturbance while experiencing loss of energy (based on the surface wind speed) and amplitude (based on microbarograph data) along the way. Prefrontal sounding data reveals that strong low level opposing flow is the most obvious energy trapping mechanism operating in this case which allows the observed waves to be maintained for several periods.

Comparisons are made with other observations, and an alternative interpretation for thunderstorm cold outflow cases with embedded wind surges is justified. In the past the "multiple surge" phenomena was attributed to pulsating downdrafts and/or Kelvin–Helmholtz shear instabilities on the upper surface of the density current. The alternative interpretation of a developing solitary wave family presented here based on the observations from the 9 May 1981 case is also equally justified. Many multiple surge events have occurred during the night when boundary-layer radiation inversions would naturally serve as the necessary waveguide.

Laboratory simulations of density currents moving in stratified fluids have reproduced many of the features observed in the present case. Numerical models have likewise produced undular borelike disturbances which moved ahead of the density current source, although quite a bit more work remains to be done to better understand these phenomena. For example, the effects of various vertical environmental density and wind profiles on the structure and evolution of the density current and the incipient wave family is just beginning to be studied.

Acknowledgments. We express our appreciation to Dr. Douglas Christie of the Australian National University who inspired us to take a closer look at the data. We also thank the others who have reviewed this paper and provided valuable constructive insight, including Drs. A. Crook, M. Miller, J. Rottman, J. Simpson and R. Smith. We are likewise grateful to the scientists, engineers and technicians at NSSL who collected and processed these data. This work was supported under FAA Grant RM2A0702.

REFERENCES

Atlas, D., 1960: Radar detection of the sea breeze. *J. Meteor.*, **17**, 244–258.

Benjamin, T. B., 1967: Internal waves of permanent form in fluids of great depth. *J. Fluid Mech.*, **29**, 559–592.

——, 1968: Gravity currents and related phenomena. *J. Fluid Mech.*, **31,** 209–248.
Britter, R. E., and J. E. Simpson, 1978: Experiments on the dynamics of a gravity current head. *J. Fluid Mech.*, **88,** 223–240.
Charba, J., 1974: Application of gravity current model to analysis of squall-line gust front. *Mon. Wea. Rev.*, **102,** 140–156.
Christie, D. R., 1989: Long nonlinear waves in the lower atmosphere. *J. Atmos. Sci.*, **46,** 1462–1491.
——, and K. J. Muirhead, 1983: Solitary waves: A low-level wind shear hazard to aviation. *Int. J. Aviat. Safety,* **1,** 169–190.
——, —— and A. J. Hales, 1978: On solitary waves in the atmosphere. *J. Atmos. Sci.*, **35,** 805–825.
——, —— and ——, 1979: Intrusive density flows in the lower troposphere: A source of atmospheric solitons. *J. Geophys. Res.*, **84,** 4959–4970.
Clarke, R. H., 1983: Fair weather nocturnal inland wind surges and atmospheric bores. Part II: Internal atmospheric bores in northern Australia. *Aust. Meteor. Mag.*, **31,** 147–160.
——, 1984: Colliding sea breezes and the creation of internal atmospheric bore waves: Two-dimensional numerical studies. *Aust. Meteor. Mag.*, **32,** 207–226.
——, R. K. Smith and D. G. Reid, 1981: The morning glory of the Gulf of Carpentaria: An atmospheric undular bore. *Mon. Wea. Rev.*, **109,** 1726–1750.
Crook, N. A., 1986: The effect of ambient stratification and moisture on the motion of atmospheric undular bores. *J. Atmos. Sci.*, **43,** 171–181.
——, 1988: Trapping of low-level internal gravity waves. *J. Atmos. Sci.*, **45,** 1533–1541.
—— and M. J. Miller, 1985: A numerical and analytical study of atmospheric undular bores. *Quart. J. Roy. Meteor. Soc.*, **111,** 225–242.
Doviak, R. J., and R. Ge, 1984: An atmospheric solitary gust observed with a Doppler radar, a tall tower and a surface network. *J. Atmos. Sci.*, **41,** 2559–2573.
Droegemeier, K. K., and R. B. Wilhelmson, 1987: Numerical simulation of thunderstorm outflow dynamics. Part I: Outflow sensitivity experiments and turbulence dynamics. *J. Atmos. Sci.*, **44,** 1180–1210.
Goff, R. C., 1976: Vertical structure of thunderstorm outflows. *Mon. Wea. Rev.*, **104,** 1429–1440.
——, 1977: Some observations of thunderstorm-induced low-level wind variations. *J. Aircraft,* **14,** 423–427.
Haase, S. P., and R. K. Smith, 1984: Morning glory wave clouds in Oklahoma: A case study. *Mon. Wea. Rev.*, **112,** 2078–2089.
—— and ——, 1989a: The numerical simulation of atmospheric gravity currents. Part I: Neutrally-stable environments. *Geophys. Astro. Fluid Dyn.*, in press.
—— and ——, 1989b: The numerical simulation of atmospheric gravity currents. Part II: Environments with stable layers. *Geophys. Astro. Fluid Dyn.*, in press.
Ligda, M. G. H., and S. G. Bigler, 1958: Radar echoes from a cloudless cold front. *J. Meteor.*, **15,** 494–501.
Maxworthy, T., 1980: On the formation of nonlinear internal waves from the gravitational collapse of mixed regions in two and three dimensions. *J. Fluid Mech.*, **96,** 47–64.
Middleton, G. V., 1966: Experiments on density and turbidity currents. I: Motion of the head. *Canadian J. Earth Sci.*, **3,** 523–546.
Mitchell, K. E., and J. B. Hovermale, 1977: A numerical investigation of a severe thunderstorm gust front. *Mon. Wea. Rev.*, **105,** 657–675.
Mueller, C. K., and R. E. Carbone, 1987: Dynamics of a thunderstorm outflow. *J. Atmos. Sci.*, **44,** 1879–1898.
National Oceanic and Atmospheric Administration, 1981: *Storm Data,* National Climatic Data Center, Asheville, NC.
Noonan, J. A., and R. K. Smith, 1985: Linear and weakly nonlinear internal wave theories applied to "morning glory" waves. *Geophys. Astro. Fluid Dyn.*, **33,** 123–143.
——, and ——, 1986: Sea-breeze circulations over Cape York Peninsula and the generation of Gulf of Carpentaria cloud line disturbances. *J. Atmos. Sci.*, **43,** 1679–1693.
Pothecary, I. J. W., 1954: Short-period variations in surface pressure and wind. *Quart. J. Roy. Meteor. Soc.*, **80,** 395–401.
Rottman, J. W., and J. E. Simpson, 1989: The formation of internal bores in the atmosphere: a laboratory model. *Quart. J. Roy. Meteor. Soc.*, **115,** 941–963.
Scott, R. W., and B. Ackerman, 1983: Surface signatures of a dry nocturnal gust front. *Mon. Wea. Rev.*, **111,** 197–204.
Shreffler, J. H., and F. S. Binkowski, 1981: Observations of pressure jump lines in the Midwest, 10–12 August 1976. *Mon. Wea. Rev.*, **109,** 1713–1725.
Simpson, J. E., 1969: A comparison between laboratory and atmospheric density currents. *Quart. J. Roy. Meteor. Soc.*, **95,** 758–765.
——, 1972: Effects of the lower boundary on the head of a gravity current *J. Fluid Mech.*, **53,** 759–768.
——, 1982: Gravity currents in the laboratory, atmosphere, and ocean. *Ann. Rev. Fluid Mech.*, **14,** 213–234.
——, and R. E. Britter, 1980: A laboratory model of an atmosperic mesofront. *Quart. J. Roy. Meteor. Soc.*, **106,** 485–500.
Smith, R. K., 1988: Travelling waves and bores in the lower atmosphere: The "morning glory" and related phenomena. *Earth Sci. Rev.*, **25,** 267–290.
——, and B. R. Morton, 1984: An observational study of north-easterly "morning glory" wind surges. *Aust. Meteor. Mag.*, **32,** 155–175.
Tepper, M., 1950: A proposed mechanism of squall lines: The pressure jump line. *J. Meteor.*, **7,** 21–29.
Thorpe, A.J., M.J. Miller and M.W. Moncrieff, 1980: Dynamical models of two-dimensional downdraughts. *Quart. J. Roy. Meteor. Soc.*, **106,** 463–484.
Wakimoto, R. M., 1982: The life cycle of thunderstorm gust fronts as viewed with Doppler radar and rawinsonde data. *Mon. Wea. Rev.*, **110,** 1060–1082.
Wood, I. R., and J. E. Simpson, 1984: Jumps in layered miscible fluids. *J. Fluid Mech.*, **140,** 329–342.
Zrnić, D. S., and J. T. Lee, 1983: Investigation of the detectability and lifetime of gust fronts and other weather hazards to aircraft. FAA Rep. No. DOT/FAA/PM-83/33, Dep't of Transportation, 58 pp. [Available through NTIS, Springfield, VA 22151, NTIS No. AD-A141 552].